## Effects of strong electron correlations and van der Waals interactions in the physical properties of bulk and 2D FeCl<sub>2</sub>

Sinhué López-Moreno<sup>a,b,\*</sup>, Andres Tellez-Mora<sup>c</sup>, Jose Mejía-López<sup>d</sup>, Esther Elena Hernández-Vázquez<sup>b,e</sup>, Aldo H. Romero<sup>c,f</sup> and Jose Luis Morán-López<sup>b,g</sup>

#### ARTICLE INFO

# Keywords: TMDH compounds First-principles calculations Electronic structure Mechanical stability Magnons Spintronics

#### ABSTRACT

We conducted a first-principles study of FeCl<sub>2</sub>, focusing on the significance of strong electron correlations using the GGA+U approximation and van der Waals (vdW) interactions to enhance its physicochemical properties description. Our results provide an excellent characterization of both the bulk CdCl<sub>2</sub>-type structure and the 2D phase 1T crystal structure. We found that both phases were elastically and dynamically stable, showing good agreement with the experimental data from IR, Raman, inelastic neutron scattering, and magnetic measurements. The impact of the FeCl<sub>2</sub> dimensionality is discussed in detail. Additionally, we investigated the less-explored distorted 1T phase (1T'), where structural distortions introduce anisotropies that notably affect its properties, particularly its semiconducting behavior. Moreover, our analysis of the magnon spectrum aligns with the recently characterized magnetic properties of the FM 1T phase. Simultaneously, magnetic anisotropy calculations revealed that the 1T' configuration exhibits greater stability in the presence of an external magnetic field.

#### 1. Introduction

Recently, interest has increased significantly in the synthesis and theoretical exploration of novel structures with reduced dimensionality. The remarkable success of isolating graphene drove this surge, including the characterizations and different studies performed on graphene [1]. The controlled isolation of graphene has paved the way for synthesizing and characterizing more complex two-dimensional (2D) materials such as the 2D transition-metal chalcogenides (TMDs) [2] and TM dihalides (TMDHs) [3]. These materials exhibit fascinating physical and chemical properties, offering the potential for various technological applications. Examples of such applications include optoelectronic devices, magnetotransport devices, electrocatalysts, photovoltaic devices, field-effect transistors, and topological insulators [4–6].

FeCl<sub>2</sub>, along with other transition TMDHs [7], forms ferromagnetic (FM) layered structures held together by van

ORCID(s): 0000-0001-6292-8275 (S. López-Moreno); 0000-0002-3080-5868 (A. Tellez-Mora); 0000-0003-0301-3408 (J. Mejía-López); 0000-0001-7340-6456 (E.E. Hernández-Vázquez); 0000-0001-5968-0571 (A.H. Romero); 0000-0003-1472-4264 (J.L. Morán-López) der Waals interactions [8], see Fig. 1 (a). This makes it possible to isolate the bulk material into units consisting of an iron layer sandwiched between two chloride layers, using techniques similar to those employed by experimentalists for other comparable materials [9]. After exfoliation, layered materials' electronic and magnetic properties can offer new opportunities for creating heterostructures [3, 10, 11]. Only recently, it was possible to synthesize nanometer-size thin FeCl<sub>2</sub> films on highly oriented pyrolytic graphite (HOPG) by molecular-beam epitaxy (MBE) [12]. However, MBE and mechanical exfoliation techniques usually feature small areas, uncontrollable layer numbers, high costs, and harsh experimental conditions [13]. On the other hand, Jiang et al. used chemical vapor deposition (CVD) to grow highquality 2D TMDHs flakes (1T-FeCl<sub>2</sub>, -FeBr<sub>2</sub>, -VCl<sub>2</sub>, and -VBr<sub>2</sub>) on SiO<sub>2</sub>/Si. At the same time, monolayers of FeCl<sub>2</sub> on graphene/Cu foil were obtained [13]. Besides the synthesis, the study was accompanied by the structural, optic, magnetic, and vibrational characterization of the FeCl<sub>2</sub> monolayer, giving new evidence about TMDHs to validate previous theoretical reports. In this sense, first-principles calculations have been used to study the 1H, 1T, and 1T' phases of the 2D FeCl<sub>2</sub> [14–19]. Since FeCl<sub>2</sub> exhibits vdW interactions in the stacking direction [8], it is expected that there will be a significant similarity in the properties of the isolated 1T phase and the individual FeCl<sub>2</sub> layers from the bulk, see Fig. 1. However, there are significant differences

a CONACYT - División de Materiales Avanzados, IPICYT, Camino a la presa de San José 2055 Col. Lomas 4a sección, San Luis Potosí 78126, México

<sup>&</sup>lt;sup>b</sup> Grupo de Ciencia e Ingeniería Computacionales, Centro Nacional de Supercómputo, IPICYT, Camino a la Presa de San José 2055 Col. Lomas 4a sección, San Luis Potosí 78216 México

<sup>&</sup>lt;sup>c</sup>Physics Department, West Virginia University, Morgantown, WV, 26506-6315, USA

<sup>&</sup>lt;sup>d</sup>Centro de Investigación en Nanotecnología y Materiales Avanzados CIEN-UC, Facultad de Física, Pontificia Universidad Católica de Chile, Santiago, Chile

<sup>&</sup>lt;sup>e</sup>Universidad Autónoma de Chihuahua (UACH), Facultad de Ciencias Químicas, Circuito Universitario S/N, Campus UACH II, Chihuahua, Chih. México. Asociado Externo del GCIC-CNS

<sup>&</sup>lt;sup>f</sup>Department of Physics and Materials Science, University of Luxembourg, 1511 Luxembourg, Luxembourg

<sup>&</sup>lt;sup>8</sup> División de Materiales Avanzados, IPICYT, Camino a la presa de San José 2055 Col. Lomas 4a sección, San Luis Potosí 78126, México

<sup>\*</sup>Corresponding author

<sup>🔊</sup> sinhue.lopez@ipicyt.edu.mx (S. López-Moreno)

https://www.ipicyt.edu.mx/curricular/SinhuéLópezMoreno (S. López-Moreno)

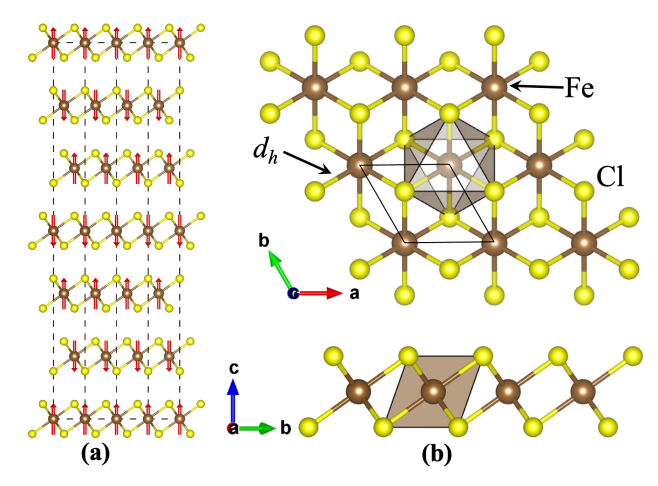


**Figure 1:** Crystalline structure of the (a) antiferromagnetic (AFM) bulk  $FeCl_2$  and (b) the FM 2D layered 1T phase. The 1T' phase is a distorted version of 1T, where the structural differences between 1T and 1T' are so small that they cannot be seen with the naked eye. Small yellow and large brown spheres represent Cl and Fe, respectively. We used the VESTA software [24] to build the structures.

between the theoretical results from the 1T phase and those reported experimentally for the bulk [8, 20–23] and the monolayer [13].

The purpose of the present research is two-fold: first, to improve the theoretical description of bulk FeCl<sub>2</sub> and second, to determine the physicochemical properties of the isolated 2D layer system in the 1T and 1T' phases: structural stability, electronic, magnetic, vibrational, elastic, and mechanical properties by using first-principles calculations.

The paper is structured as follows: In the next section, we outline the computational procedure employed in this work. Subsequently, we present the results and discuss the structural, electronic, vibrational, elastic, mechanical, and magnetic properties of the bulk and 2D FeCl<sub>2</sub> in Sections 3.1 and 3.2, respectively. Finally, we summarize and conclude in Section 4.

#### 2. Computational details

The calculations of the total energy were performed within the framework of the density functional theory (DFT) and the projector-augmented wave (PAW) [25, 26] method, as implemented in the Vienna *ab initio* simulation package (VASP) [27–30]. We used a plane-wave energy cutoff of 400 eV. The exchange-correlation energy was described within the generalized gradient approximation (GGA) in the Perdew-Burke-Ernzerhof (PBE) formulation [31]. We considered fourteen valence electrons for Fe  $(3p^6 \ 4s^1 \ 4d^7)$  and seven valence electrons for Cl  $(3s^2 \ 3p^5)$  in the PAW pseudopotential. The GGA+U approximation has been used within the Dudarev's approach  $(U_{\rm eff} = U \ - J^{\rm H})$  [32] to account for the strong d-orbital correlation. This method has been used successfully in studying other  $AX_2$  compounds [33–35]. In this work, we have used U = 6 eV and  $J^{\rm H} = 0.95$ 

eV for Fe atoms ( $U_{\rm eff}=5.05$  eV). We chose these values in order to find an equilibrium between the results obtained from the electronic structure, the structural parameters, and the phonons with the experimental values from the literature. On the other hand, similar values were used with relative success in the study of other Fe-based compounds [33, 36–42]. We also considered vdW interactions to account for the long-range forces in bulk and 2D FeCl<sub>2</sub> [43–53]. A detailed evaluation of the structural parameters as a function of the different vdW methods is discussed in the following section. Our calculations also include the non-spherical contributions related to the density gradient in the PAW spheres.

The Γ-centered Monkhorst-Pack scheme was employed for the Brillouin-zone (BZ) integrations [54] with mesh  $11\times11\times1$ , corresponds to a set of 16 special k-points in the irreducible BZ for bulk and 2D system. However, we use a denser mesh for each case of the electronic structure calculations. The chosen cutoff energy and k-mesh ensure that in the relaxed equilibrium configuration, the energy is converged to  $1\times10^{-7}$  eV, and the forces are less than one meV/Å per atom in each Cartesian direction. The highly converged results on forces are required to calculate the dynamical matrix using the direct force constant approach [55]. This method allows us to identify the irreducible representation and the character of the phonon modes at the zone center ( $\Gamma$  point). The elastic tensor is determined by performing six finite lattice distortions and deriving the elastic constants from the strain-stress relationship [56], as is discussed in Ref. [57]. The calculations of the 2D FeCl<sub>2</sub> were done in a cell that contains 17 Å of vacuum to avoid spurious interaction between neighboring cells.

The majority of the magnetic property calculations were carried out using the SIESTA code [58], which employs a linear combination of atomic orbitals (LCAO) method. We opted for a different package for these calculations primarily due to SIESTA's use of a localized basis set, which is particularly advantageous when applying a Green's function approach to compute magnetic properties. In contrast, with VASP, one alternative is constructing a localized Hamiltonian using Maximally Localized Wannier Functions (MLWFs). However, this method is highly sensitive to the chosen energy window, making it challenging for a large number of calculations. For a more detailed discussion of this approach and its application in determining the magnetic ground state, refer to reference [59]. Additionally, the magnetic perturbations and the Heisenberg model fitting are done using the TB2J code [60], which uses a single-particle Green's function method. Calculations with SIESTA were done within the GGA+U approximation with the same Uand J parameters used in the VASP calculations. In addition, we used the norm-conserving scalar-relativistic pseudopotentials taken from the PSEUDO-DOJO periodic table [61] with the PBE exchange-correlation functional and a doblezeta polarized LCAO basis along with a 400 Ry cutoff energy. Bulk calculations were done with the vdW density functional correction given by Klimes-Bowler-Michaelides [62].

**Table 1** Theoretical results of the ground-state lattice parameters for the AFM bulk  $FeCl_2$  using GGA+U and GGA+U plus the vdW approximations, see the description in the text. We included the experimental results from Ref. [8] for comparison. Here, a and c are the lattice constants, and V is the equilibrium volume.

	a (Å)	c (Å)	c/a	V (Å <sup>3</sup> )
$\overline{GGA + U}$	3.6023	18.7588	5.2074	210.81
D2	3.5359	17.5847	4.9731	190.40
D3	3.5769	17.3968	4.8636	192.76
D3'	3.5460	17.3076	4.8809	188.47
TS	3.5941	17.5610	4.8881	196.53
SCS	3.5667	17.3844	4.8741	191.53
HI	3.5921	18.1214	5.0448	202.50
DF	3.6697	17.8921	4.8756	208.67
DF2	3.5522	17.2739	4.8628	188.77
oPBE	3.6706	17.9145	4.8805	209.03
oB88	3.5725	17.2422	4.8264	190.58
oB86b	3.5449	17.2725	4.8724	187.97
Exp. [8]	3.5980	17.5360	4.8738	196.60

#### 3. Results and Discussion

The labels are explained in the text.

#### **3.1. Bulk**

#### 3.1.1. Crystalline structure

At ambient conditions, FeCl<sub>2</sub> crystallizes in the CdCl<sub>2</sub>-type structure [space group (SG):  $R\bar{3}m$ , No. 166] [8]. In the primitive rhombohedral cell (Z=1), Fe atoms occupy the Wyckoff position (WP) 1a (0, 0, 0), while Cl is in the WP 2c (x, x, x) with  $x=0.2543\pm0.0005$  [23]. On the other hand, in the hexagonal setting (Z=3), Fe atoms are in the WP 3a (0, 0, 0) and Cl in the WP 6c (0, 0, z) with z close to 0.25, see Fig. 1 (a). Here, Fe atoms are six coordinated with Cl ions forming almost perfect FeCl<sub>6</sub> octahedra, distorted due to Jahn-Teller effect [63], sharing edges with other FeCl<sub>6</sub> units, to form FM layers in the xy plane. The layers in the z axis are stacked in an ABC sequence with an antiferromagnetic (AFM) order along this axis. Thus, the whole magnetic structure requires considering a double hexagonal cell in the [001] direction to describe the AFM phase correctly [23].

From the theoretical point of view, the standard calculations with GGA+U, but without vdW interaction, yield a lattice parameter a=3.6023~Å (hexagonal setting) in agreement with the experimental value of 3.5980 Å[8]. However, this approximation fails to describe the long-range bonding in the stacking direction and predicts a value of c=18.7588~Å, which is  $\approx 7\%$  larger than the experimental one [8]. Also, it is essential to mention that calculations with only GGA approximation, not taking account of the U interaction, underestimate the lattice parameter a (3.518 Å) and overestimate c (19.149 Å). Thus, it is crucial to consider an approximation that can reproduce the experimental results for the laminar structure and the long-range interactions in the [001] direction.

In order to use the best option to consider long-range interactions, we performed a systematic minimization energy

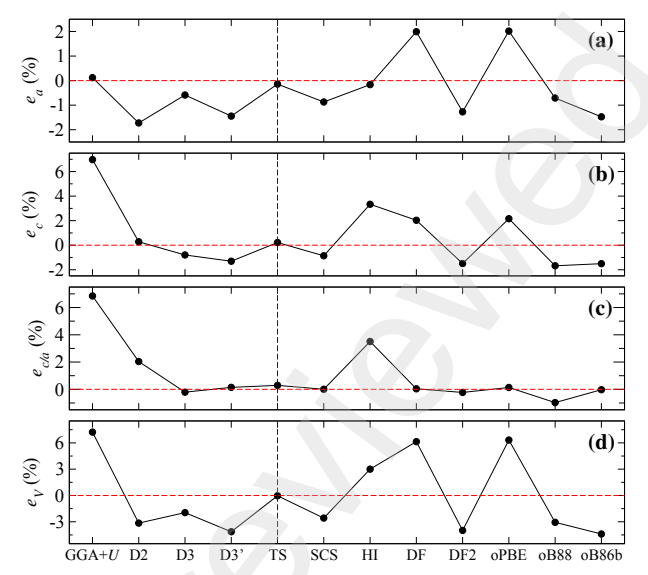


**Figure 2:** Difference between the experimental and the calculated values  $[e_x(\%)]$  by using GGA+U and GGA+U plus the vdW approximations; see the description in the text. The four panels correspond to the difference in the lattice parameters (a) a ( $e_a$ ), (b) c ( $e_c$ ), (c) the c/a ratio ( $e_{c/a}$ ), and (d) volume ( $e_V$ ) for the AFM bulk FeCl<sub>2</sub>. The error is measured against the experimental values from Ref. [8]; see Table 1. The vertical blue dashed lines correspond to the results with the slightest overall difference.

calculations series of bulk FeCl<sub>2</sub> with GGA+U and most of the available options from the VASP code. We considered the D2 method of Grimme [43], zero damping D3 method of Grimme [44], D3 method with Becke-Jonson damping (D3') [64], Tkatchenko-Scheffler method (TS) [45], the self-consistent screening in TS method (SCS) [65], the TS method with iterative Hirshfeld partitioning (HI) [46], the vdW-DF method introduced by Dion (DF) [47], the vdW-DF2-B86R method (DF2) [53], the optPBE (oPBE), optB88 (oB88), and the optB86b (oB86b) [49, 51, 52]. From this point on, we omit to mention the GGA+U approximation for these calculations, and we only use the standard acronym used in the mentioned vdW approximations. The optimized volume and lattice parameters for bulk FeCl2 and the experimental data from Ref. [8] are listed in Table 1. As we can see, there are significant differences among the various approximations.

To better illustrate the results using different methods and approximations, we show in Figure 2 the difference between the calculated values and the experimental results for lattice parameters (a) a ( $e_a$ ), (b) c ( $e_c$ ), (c) the c/a ratio ( $e_{c/a}$ ), and (d) volume ( $e_V$ ). After considering the four parameters, the best choice is the TS approximation, followed by D3 and SCS. The error is less than 0.3 % for lattice parameters and volume for the first one. Thus, we use the TS approximation in all the calculations. It is worth mentioning that this approximation was also successful in studying graphene interacting with a MoS<sub>2</sub> monolayer [66].

The Fe–Cl bond length obtained with the TS approximation in the present study is 2.4919 Å, very similar to the experimental result  $d_{\rm Fe-Cl}=2.488$  Å [8]. Furthermore, the FeCl<sub>2</sub>–FeCl<sub>2</sub> interlayer distance, 3.0965 Å, also agrees with the experimental value of 3.088 Å [8]. Thus, the TS approximation reproduces the crystallographic values of the FeCl<sub>2</sub> compound in the periodic three-atomic layer and the long-range interaction along the perpendicular direction.

#### 3.1.2. Electronic structure

Regarding the electronic structure, it was reported in the literature that a single crystal of FeCl<sub>2</sub> presents a direct energy band-gap of 8.48 eV from reflectivity measurements using synchrotron radiation [67]. We followed the band structure calculations in the A- $\Gamma$ -M-K- $\Gamma$  path and the electronic density of states (DOS) with the GGA+U approximation plus the vdW interaction. The A- $\Gamma$  path indicates the band dispersion between layers, while the  $\Gamma$ -M-K- $\Gamma$  path shows the band dispersion on the xy plane. Figure 3 shows the band structure and DOS for the FeCl<sub>2</sub> crystal, where the zero energy corresponds to the Fermi level. FeCl<sub>2</sub> presents an indirect energy band-gap  $(E_g)$  of 3.62 eV from the  $\Gamma$ -M to the M point, which could be larger if hybrid functionals are used to obtain  $E_{\varrho}$  [14]. The valence band maxima (VBM) is mainly occupied by  $3d_{72}$  and  $3p_{7}$  states from Fe and Cl, respectively. At the same time, the conduction band minima (CBM) is filled with  $3d_{vz}$  and  $3d_{x^2-v^2}$  states. Note that bands in the A- $\Gamma$  path in the band structure around the Fermi level are almost flat, i.e., there is no dispersion in the bands along the z-axis. This indicates a weak interaction between layers, which is a signature of the 2D nature of this compound. Thus, the electronic conduction is along the xy plane. The bands contributing to the electron transport are Fe- $e_q$  states with contributions from  $p_z$  states and dispersion of  $\approx 0.214$ eV (measured as the electron bandwidth around the Fermi energy).

It is important to note that if the magnetic moment is defined through the polarization of the integrated charge per spin channel with a Wigner-Seitz radius of 1.164 Å, the predicted magnetic moment value is 3.72  $\mu_{\rm B}$ , smaller than the reported experimental value of  $4.5\pm0.7~\mu_{\rm B}$  [68]. However, recently it has been reported that magnetic moment is composed of spin and orbital contributions, being 3.56  $\mu_{\rm B}$  from spin and 0.59  $\mu_{\rm B}$  from the orbital along the z axis [17]. Hence, our results are in agreement with previous results from the spin moment.

#### 3.1.3. Phonon spectra and mechanical stability

We calculated the phonon spectra and the elastic constants in order to determine the dynamical and elastic stability of bulk FeCl<sub>2</sub>. According to the group theory, the FeCl<sub>2</sub> (SG:  $R\bar{3}m$ ) has the following phonon Raman (R) and infrared (IR) phonon modes at the  $\Gamma$  point:  $\Gamma = 2A_{2u}(IR) + 2E_u(IR) + E_g(R) + A_{1g}(R)$ . One  $A_{2u}$  and one  $E_u$  modes are acoustic, and the rest are optic. The double degenerated  $E_g$  and  $E_u$  modes correspond to vibrations on the plane, while the non-degenerated modes  $A_{1g}$  and  $A_{2u}$  are produced

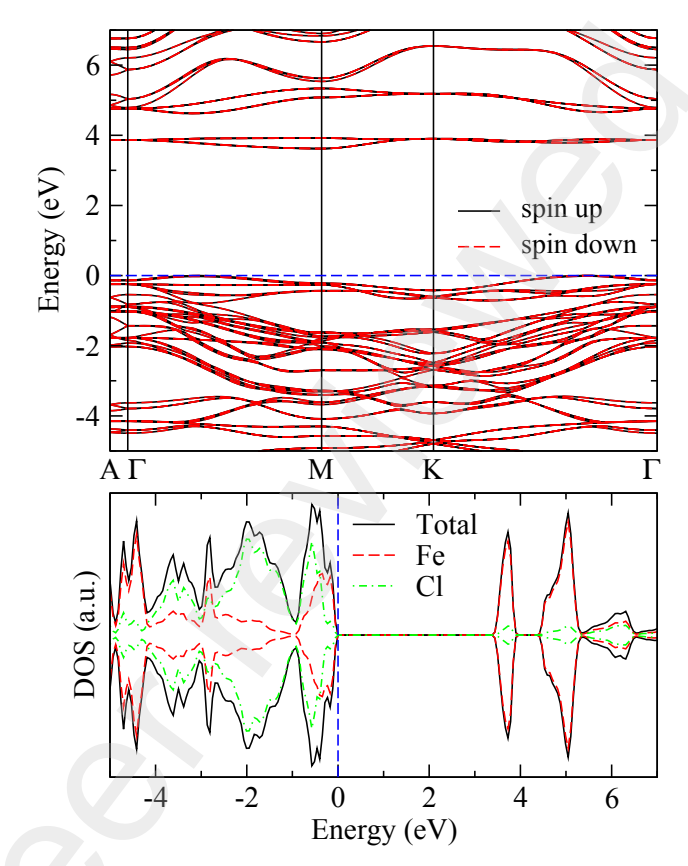
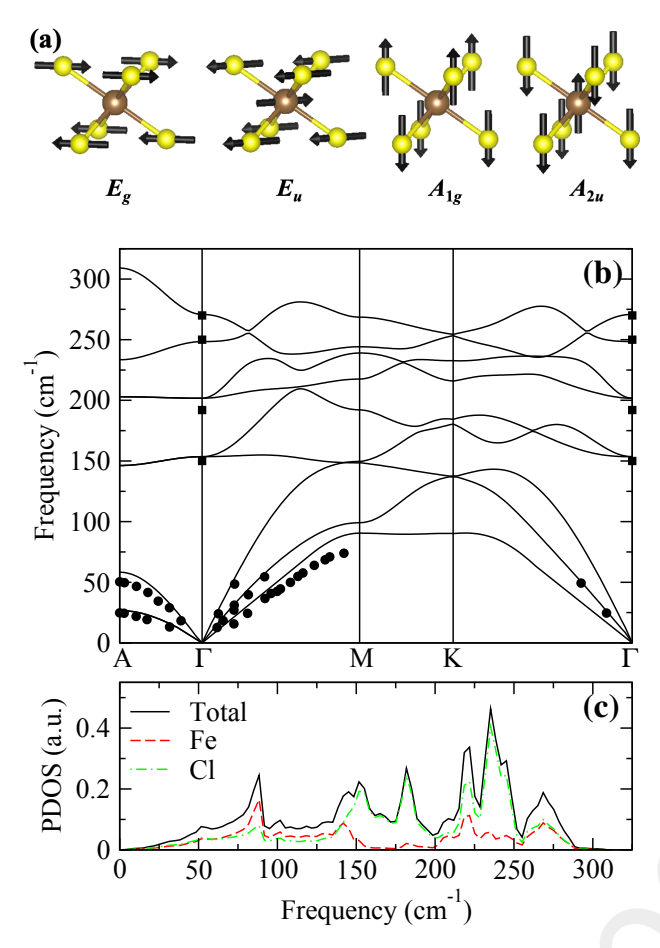


Figure 3: (a) Band structure and (b) density of states (DOS) for the AFM bulk FeCl<sub>2</sub>. Blue dashed lines at 0 eV correspond to the Fermi level.

by vibrations of the atoms in the [001] direction, see Fig. 4 (a). As we can see, in the Raman modes, only the Cl atoms vibrate, whereas in IR modes, both Fe and Cl atoms in FeCl<sub>6</sub> octahedra do, but in opposite directions. We found that the values for the  $E_g$ ,  $E_u$ ,  $A_{1g}$ , and  $A_{2u}$  phonon modes at the  $\Gamma$  point are: 154.1, 196.1, 249.3, and 274.9 cm<sup>-1</sup>, in good agreement with the experimental values: 150, 192, 250, and 270 cm<sup>-1</sup> [20], respectively. It is worth mentioning that calculations without vdW interactions produce an error in the phonon frequencies of 8.3% compared to experimental values; this confirms the importance of including an appropriate description of the van der Waals interactions in the model.

The phonon dispersion and phonon density of states (PDOS) for bulk  $\operatorname{FeCl}_2$  are shown in Figures 4 (b) and (c), respectively. The phonon spectra include the experimental frequencies at  $\Gamma$  point reported in Ref. [20], and the acoustic phonon dispersion branches are those obtained from inelastic neutron scattering measurements [21]. As we can see, only branches with positive frequencies are present, which means the system is dynamically stable. Also, notice that there is good agreement with the experimental results [20, 21]. The A- $\Gamma$  path indicates the phonon dispersion between layers, while the  $\Gamma$ -M-K- $\Gamma$  path shows the phonon dispersion on the xy plane. Due to their weak interaction, the inter-layer dispersion is smaller than the one on the layer.



**Figure 4:** (a) Lattice vibrations producing the Raman and IR modes, (b) phonon spectra, and (c) phonon density of states (PDOS) for the AFM bulk FeCl<sub>2</sub>. Experimental data were taken from Refs. [20] (squares) and [21] (circles).

According to the A– $\Gamma$  path, the on-plane  $E_g$  and  $E_u$  phonon modes are almost unaffected by the interplanar interactions, whereas the opposite occurs for the interlayer  $A_{1g}$  and  $A_{2u}$  modes. Benedek and Frey [20] did not observe the dispersive behavior in the  $A_{1g}$  and  $A_{2u}$  phonon modes in their study based on the extended-shell method, reported in the early '80s. According to the phonon DOS, the vibrations come from both ions in all the frequency ranges, but below (above) 150 cm<sup>-1</sup>, Fe (Cl) contributes the most due to the mass difference.

Only a few reports of theoretical and experimental results regarding elastic stability exist. It is important to note that those do not include information on all the elastic constants [20, 21, 69]. According to the crystal classification, the trigonal space group No. 166 belongs to the R<sub>I</sub> Laue group, which has only six independent elastic constants:  $c_{11}$ ,  $c_{33}$ ,  $c_{44}$ ,  $c_{12}$ ,  $c_{13}$ , and  $c_{14}$  [70]. The  $c_{11}$  and  $c_{33}$  ( $c_{44}$ ) elastic constants arise from pure compression (shear) strain related to the longitudinal compression (shear modulus). The  $c_{12}$  and  $c_{13}$  elastic constants are related to the transverse expansion. In contrast, the  $c_{14}$  elastic constant mixes compression and shear strain. Furthermore, the  $c_{66} = (c_{11} - c_{12})/2$ ; thus it is not

Table 2

Upper part. Elastic constants  $c_{ij}$  (GPa) for the AFM bulk FeCl<sub>2</sub>. We include the experimental results from the literature for comparison. Lower part. Calculated mechanical properties with the VRH method from the elastic constants: B is the bulk modulus (GPa), G is the shear modulus (GPa), G is Young's modulus (GPa), G is Poisson's ratio, G0 is Pugh's ratio, and G1 is the Vickers hardness (GPa). †This work.

$c_{11}$	$c_{33}$	$c_{44}$	$c_{66}$	$c_{12}$	$c_{13}$	$c_{14}$	Ref.
71.60	32.29	5.91	23.17	25.27	12.76	1.68	†
61	22	5.0	26		13	6.6	[20]
66.3±3	$16.9 \pm 1.3$			26.9±4			[21]
	27.1	17.8	21.5				[22]
$\boldsymbol{B}$	$\boldsymbol{G}$	$\boldsymbol{E}$	ν	B/G	$H_{ m V}$		
28.08	12.66	33.02	0.30	2.22	2.24		†

an independent elastic constant. However,  $c_{66}$  is sometimes reported in experimental results. Hence, we include this elastic constant in our results to compare our data with the experiments.

As observed from Table 2, our theoretical results are in fair agreement with the experimental ones. However, we must note significant differences between the experimental values from Refs. [21] and [22]. According to Ref. [71], crystals belonging to the R<sub>1</sub> Laue group have to meet the following conditions to determine their elastic stability:  $c_{11} > |c_{12}|$ ,  $c_{44} > 0$ ,  $c_{13}^2 < c_{33}(c_{11} + c_{12})/2$ ,  $c_{14}^2 < c_{44}(c_{11} - c_{12})/2 \equiv c_{44}c_{66}$ , and  $c_{44} > 0$ . Our results from Table 2 meet the established criteria, meaning this structure is elastically stable.

The elastic response of the FeCl<sub>2</sub> compound is described by its mechanical properties. The bulk modulus (B) and shear modulus (G) can be obtained from the elastic constants  $c_{ij}$  using the Voight-Reuss-Hill (VRH) average method [72, 73], already implemented in VASPKIT [74]. The Pugh's ratio, Young's modulus (E) and Poisson's ratio (v) can be obtained as: B/G, E = 9BG/(3B + G), and v = (3B - G)(2G)/(6B+2G), respectively. Otherwise, a modification of the Chen's model [75] proposed by Tian et al. has been used to obtain the Vickers hardness:  $H_V = 0.92k^{1.137}G^{0.708}$ (k = G/B) [76]. Table 2 lists the values of B, G, E, v, B/G, and  $H_{\rm V}$  obtained with the VRH method. As we can see, FeCl<sub>2</sub> presents small values for their mechanical properties due to the crystal exhibiting weak long-range interactions in the [001] direction. Therefore, a significant anisotropy is to be expected in the mechanical properties.

To better understand the mechanical properties, the first row of Fig. 5 shows a 3D representation of B, G, E, and v, obtained with the ElATools program [77]. The second and third rows show 2D representations of the mechanical properties as a function of the  $\phi$  and  $\theta$  angles in the xy and xz planes, respectively. Mechanical properties of FeCl<sub>2</sub> are much more isotropic in the xy than in the xz plane. Also, Fig. 5 shows the clear difference between the average values from Table 2 and the directional ones observed in

Effects of strong electron correlations and van der Waals interactions in the physical properties of bulk and 2D FeCl<sub>2</sub>

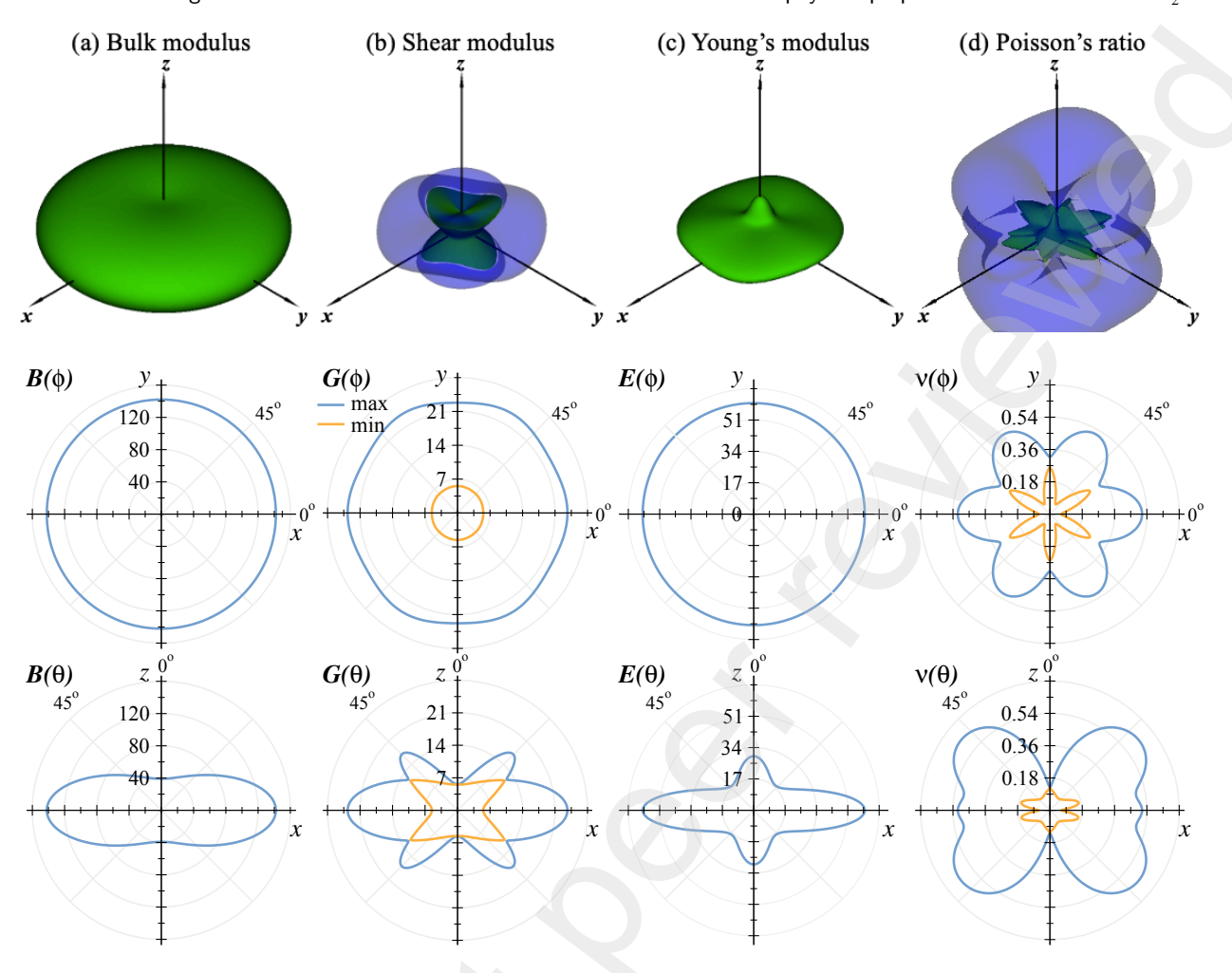


**Figure 5:** 3D and 2D representations of the mechanical properties of AFM bulk  $FeCl_2$ : (a) bulk modulus (B), (b) shear modulus (G), (c) Young's modulus (E), and (d) Poisson's ratio ( $\nu$ ), as a function of  $\phi$  and  $\theta$ , in the 3D space (upper figure) and the projections on the xy (middle figure) and xz (lower figure) planes. The units for B, G, and E are GPa,  $\nu$  is unitless. In (b) and (d), the transparent outer layer represents the maximum values, and the non-transparent inner layer represents the minimum values.

the 2D and 3D representations. The maximum value of B  $(B_{\rm max})$  is 142.06 GPa in the xy plane for all  $\phi$ , while the minimum ( $B_{min}$ ) value is 39.08 GPa in the [001] direction, meaning that the crystal is much less compressible in the [100] than in the [001] direction. The  $G_{\text{max}}$  is 23.66 GPa in the [100] direction when the plane (010) plane is sheared. This is attributed to a rigid layer that cannot be deformed under shear force. As in the bulk modulus,  $G_{\min}$  (5.54 GPa) occurs in the [001] direction due to the layered nature of  $FeCl_2$ . Young's modulus behaves similarly to B in the xyplane with  $E_{\text{max}} = 60.19$  GPa, while  $E_{\text{min}} = 16.87$  GPa very close to the (110) plane for  $\theta \approx 45^{\circ}$ . In the case of Poisson's ratio,  $v_{\text{max}} = 0.67$  and  $v_{\text{min}} = 0.018$  ( $\phi = 90^{\circ}$  and  $\theta \approx 42^{\circ}$ ). These results give the anisotrpies  $(A_X = X_{\text{max}}/X_{\text{min}})$  of  $A_B$ = 3.64,  $A_G$  = 4.28,  $A_E$  = 3.65, and  $A_V$  = 33.5 for B, G, E, and  $\nu$ , respectively. We note that those values are lower than those observed in other layered materials [78, 79].

On the other hand, the brittle or ductile behavior is a mechanical property of materials that correlates with their

reversible compressive deformation and fracture ability. According to Pugh's criterion, a material is classified as brittle if B/G < 1.75 and ductile if B/G > 1.75. In our case, B/G = 2.21, indicating the ductile nature of bulk FeCl<sub>2</sub>.

### 3.2. Layered phases 1T and 1T' 3.2.1. Crystalline structure

According to the recent experimental results [13], FeCl<sub>2</sub> can display a 2D hexagonal 1T structure (space group  $P\bar{3}m1$ , No. 164, Z=1), which corresponds to the isolation of the three Cl-Fe-Cl layers from the bulk FeCl<sub>2</sub>, see Fig. 1 (b). To calculate the properties, we separate the three layers from the bulk structure in a hexagonal cell, with a vacuum space of 17 Å to avoid spurious interactions. In the optimized 1T FM structure, the lattice parameter is a=3.59 Å, which is in excellent agreement with the experimental results of the 2D system obtained by CVD (a=3.6 Å) [13] and very close to the bulk value (a=3.598 Å [8]). This implies that there is a small reconstruction in the three-monolayer. Previous theoretical studies on the 1T phase of FeCl<sub>2</sub> report values

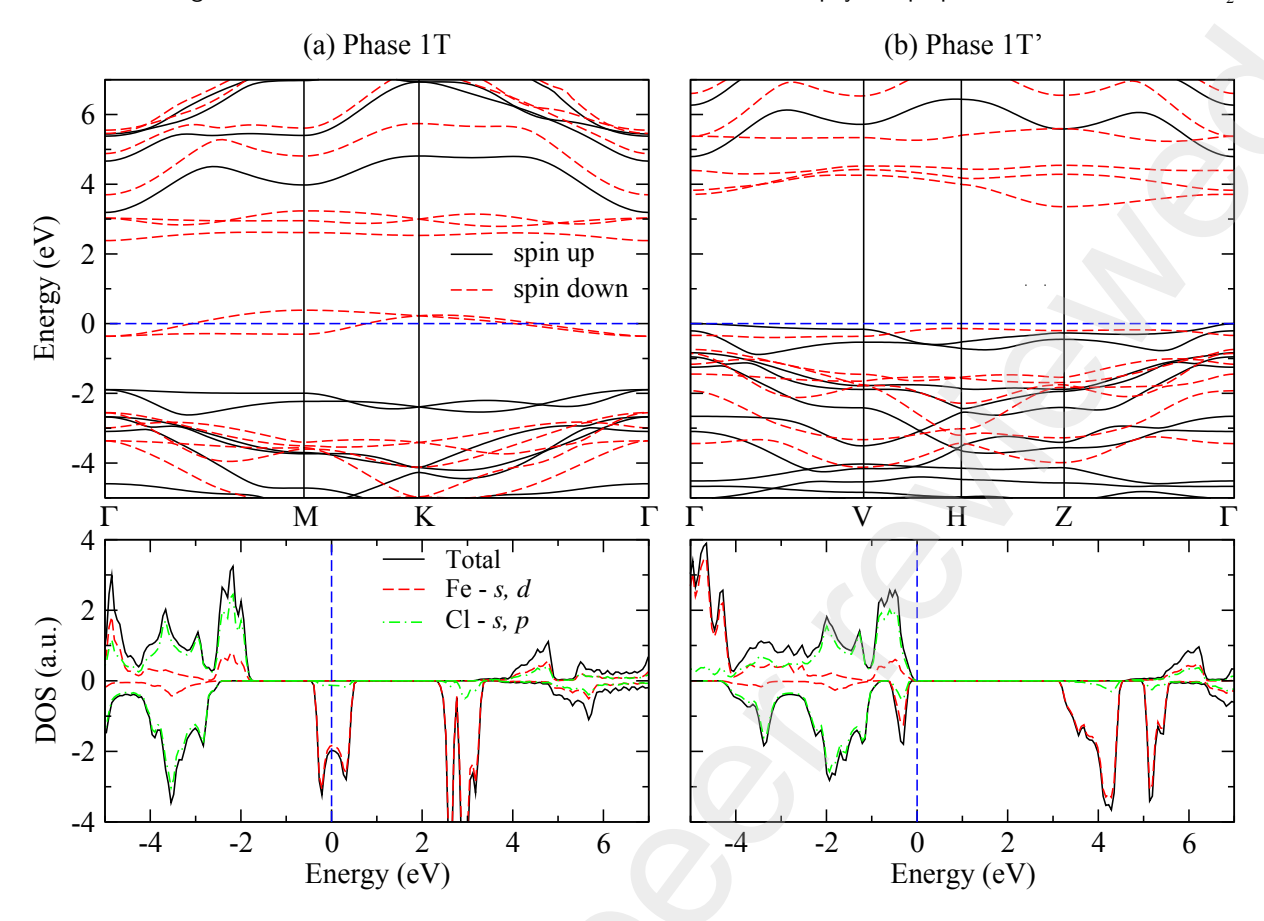


Figure 6: Band structure and density of states (DOS) for the FM 2D FeCl<sub>2</sub> in the (a) 1T and (b) 1T' phases.

between 3.41 and 3.50 Å [14–16, 19, 80]. Our results show that the Fe cation is in the WP 1b (0, 0, 1/2) and the Cl anion is in the WP 2d (1/3, 2/3, 0.56978) with the interatomic distance Fe–Cl  $d_h$  = 2.4987 Å, very close to the bulk value of 2.488 Å [8].

We used a 2×2 primitive supercell to calculate the 1T structure in the AFM configuration. Unlike the results reported in the literature [14, 15], we found that the 1T AFM structure of FeCl<sub>2</sub> is not stable; the system gets distorted and adopts a rectangular 2D structure with space group C2/m(No. 12, Z = 2), similar to the structure recently reported by Yao et al. [18]. We call this structure 1T'. This structure with the FM coupling is 3.3 meV lower in energy than the AFM one and 874 meV/f.u. lower than the hexagonal 1T FM phase. This phase is characterized by lattice parameters, a =6.355 Å, b = 3.584 Å with  $\beta = 90.071^{\circ}$  in a cell that measures 19.34 Å in the z direction. The Fe and Cl are in the WPs 2d (0, 1/2, 1/2) and 4i (0.83417, 0, 0.42756), respectively. In this structure, the FeCl<sub>6</sub> octahedra is distorted, with two interatomic Fe-Cl distances: the equatorial distance between Fe and four Cl ( $d_e = 2.5063 \text{ Å}$ ), and the apical between Fe and two Cl ( $d_a = 2.5457 \text{ Å}$ ), which are larger than  $d_h$  in the 1T phase (2.4987 Å), see Fig. 1 (b). As discussed in the next sections, the symmetry breaking and the changes in the structural parameters drastically affect all the physicochemical properties.

#### 3.2.2. Electronic structure

The electronic structure of 1T FeCl<sub>2</sub> structure has already been reported in the literature [7, 14, 15]. The HSE06 hybrid functional produced a half-metallic band structure with a spin-up energy band gap ranging from 6.4 to 6.7 eV. The same behavior was observed with GGA but with a smaller energy band gap [14]. In our case, we calculated the electronic structure along the path used in the bulk layer  $(\Gamma - M - K - \Gamma)$ . Figure 6 (a) shows the band structure and the DOS. As we can see, the band structure of the 1T phase shows the characteristics spin down bands around the Fermi level, mainly occupied by  $3d_{x^2-v^2}$  and  $3d_{xz}$  electronic states in the upper band, and  $3d_{yz}$  and  $3d_{xy}$  states for the lower band, similar to previous results [15]. On the other hand, the VBM and CBM of the spin-up states at  $\Gamma$  point are -1.89 and 3.19 eV, respectively, i.e., a spin-up band gap of 5.08 eV, close to the reported values in the literature [7, 14, 15].

The 1T' phase electronic structure presents significant differences from the 1T phase. The band structure and DOS for the 1T' phase are shown in Fig. 6 (b). Here, there is a drastic redistribution of the spin-down electronic states. The bands around the Fermi level from the 1T structure separate in the 1T'. The  $d_{xz}$  and  $d_{x^2-y^2}$  states move to energies below the Fermi level. Whereas the other band, occupied by  $d_{xy}$ ,  $d_{yz}$ , and  $d_{xz}$  states, moves up in energy, hybridizing with a higher energy band occupied with  $d_{z^2}$  states. Due

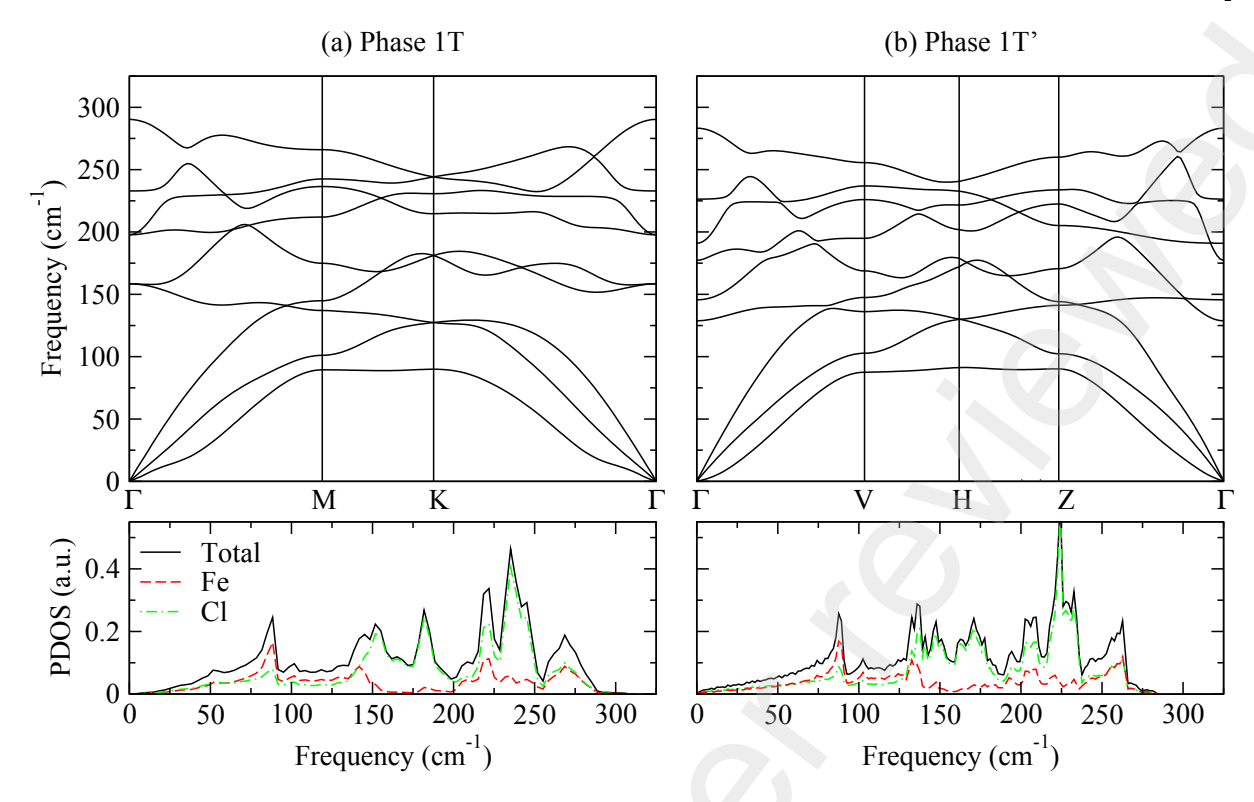


Figure 7: Phonon spectrum and phonon density of states (PDOS) for the FM 2D FeCl<sub>2</sub> in the (a) 1T and (b) 1T' phases.

to the spin-down electron redistribution, the Fermi level now falls at the border of the low energy bands, opening a gap of approximately 3.0 eV. The half-metallic conductivity reported for the 1T phase is no longer present.

According to our results, the VBM and CBM for the spin-up channel are located at  $\Gamma$  point with a direct  $\Gamma$ - $\Gamma$  energy band gap of 4.79 eV. On the other hand, the VBM and CBM are at the V-H and Z points, respectively, making an indirect energy band gap of 3.48 eV for the spin-down channel. Thus, both energy band gaps are smaller than the obtained for the 1T phase.

#### 3.2.3. Mechanical stability

As in the bulk case, we calculated the phonon spectrum and the elastic constants to determine the stability of the 2D FeCl<sub>2</sub> systems. According to the group theory, FeCl<sub>2</sub>, in the 1T structure, has the following phonon frequencies at the  $\Gamma$  point:  $\Gamma = A_{1g}(R) + 2A_{2u}(IR) + 2E_u + E_g$ . The acoustic modes are one  $A_{2u}$  and one  $E_u$ ; the rest are optic. We found the following phonon frequencies for the  $E_g$ ,  $E_u$ ,  $A_{1g}$ , and  $A_{2u}$  phonon modes: 158.5, 197.7, 232.9, and 290.3 cm<sup>-1</sup>, respectively. These frequencies are close to the values obtained in bulk and the experimental ones reported in the literature [20, 21]. On the other hand, calculations performed at the GGA level with VASP code [14] found the phonon frequencies 130, 179, 237, and 279 cm<sup>-1</sup> for  $E_g$ ,  $E_u$ ,  $A_{1g}$ , and  $A_{2u}$  modes, which differ from our results due to their computational considerations. As was expected, the eigenvectors from Raman and IR modes are the same as those observed in bulk; see Fig. 4 (a). It is worth mentioning

that Torun *et al.* [14] reported an erroneous representation of the eigenvectors for the  $A_{2u}$  IR mode. The phonon spectrum and PDOS corresponding to the 1T structure are shown in Fig. 7 (a). The phonon spectrum of the monolayer is similar to the bulk one in the  $\Gamma$ -M-K- $\Gamma$  path. However, there are some differences in  $A_{2u}$  and  $A_{1g}$  modes close to  $\Gamma$  point and in the  $\Gamma$ -M direction. This result is related to the absence of the stacking layers in the z axis.

The 1T' phase presents the following phonon modes at the  $\Gamma$  point:  $\Gamma = 2A_u(IR) + 4B_u(IR) + 2A_g(R) + B_g(R)$ . The acoustic modes are two  $B_u$  and one  $A_u$ ; the rest are optic. Due to the symmetry breaking, the  $E_{\varphi}$  mode characteristic of the 1T phase splits into the  $A_g$  and  $B_g$  modes in the 1T' phase. They have the exact nature of  $E_g$  mode, but the eigenvectors corresponding to  $A_g$  and  $B_g$  modes are in the [100] and [010] directions. Where the apical distance  $(d_a)$  is oriented in the [100] direction, while the equatorial distance  $(d_e)$  is on a plane, rotated  $\approx 30^{\circ}$  with respect to the y axis. Thus, this difference in the geometry is reflected in the phonon frequencies in these modes. Similarly, the  $E_{\mu}$  mode splits into the  $B_{\mu}$  and  $A_{\mu}$  modes, produced by vibrations in the [100] and [010] directions. The obtained frequencies are 128.5, 145.3, 177.0, 190.6, 226.1, and 283.0 cm<sup>-1</sup> for the phonon modes  $A_g$ ,  $B_g$ ,  $B_u$ ,  $A_u$ ,  $A_g$ , and  $B_u$ , respectively.

Figure 7 (b) shows the PDOS and the phonon spectrum for the 1T' phase. Since the phonon spectrum does not present any negative branches, the condition for dynamical stability for the 1T' system is observed. We can see significant similarities between the two phases because the rectangular structure is a distortion of the hexagonal one. The

Effects of strong electron correlations and van der Waals interactions in the physical properties of bulk and 2D FeCl<sub>2</sub>

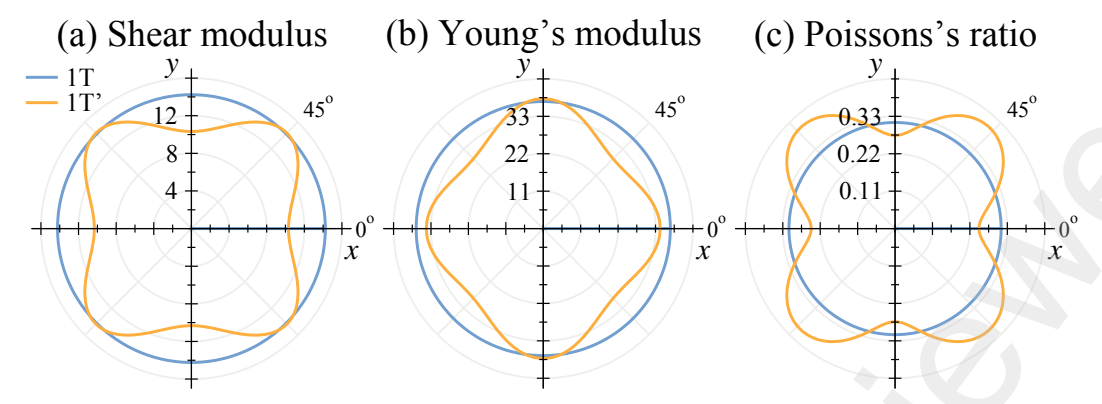


**Figure 8:** Angular dependence of the (a) shear modulus  $G(\phi)$ , (b) Young's modulus  $Y(\phi)$ , and (c) Poisson's ratio  $v(\phi)$  for the FM 2D FeCl<sub>2</sub> 1T and 1T' phases.

**Table 3** Elastic constants (in N/m) and mechanical properties for the FM 2D FeCl<sub>2</sub> and MoS<sub>2</sub>. We include theoretical and experimental results from the literature for comparison.  ${}^{a}$ Ref. [66],  ${}^{b}$ Ref. [81].  ${}^{\dagger}$ This work.

		$c_{11}$	$c_{22}$	$c_{12}$	c <sub>66</sub>	γ	$Y_{[10]}$	$Y_{[01]}$	ν <sub>[10]</sub>	$\nu_{[01]}$
FeCl <sub>2</sub>										
	1T	41.37		12.90	14.23	27.13	37.34		0.31	
	1T'	36.84	40.94	10.10	10.32	24.46	34.35	38.18	0.25	0.27
		oS <sub>2</sub> 133.0 <sup>†</sup> 132.3 <sup>a</sup>		33.00 32.8		83.2 82.5	-		0.25 0.25 0.25	

reduction of symmetry causes an increase in the dispersion of the phonon branches, which is reflected in an increasing noise in the PDOS.

The elastic constants were computed as in the bulk with the respective considerations for 2D materials [57, 66, 74]. However, since there are no experimental nor theoretical results to compare, we also calculated the elastic constants for 2D MoS<sub>2</sub> to compare with results from the literature and validate our procedure. The elastic constants for both phases of 2D FeCl<sub>2</sub> (1T:  $c_{11}$  and  $c_{12}$ ,  $c_{66} = (c_{11} - c_{12})/2$ ; 1T':  $c_{11}$ ,  $c_{22}$ ,  $c_{66}$ , and  $c_{12}$ ) and MoS<sub>2</sub> (2H:  $c_{11}$  and  $c_{12}$ ,  $c_{66}$ =  $(c_{11} - c_{12})/2$ ), are presented in Table 3. As observed, there is a good agreement between experimental and theoretical results from the literature for MoS<sub>2</sub> [66, 81]. In the case of FeCl<sub>2</sub>, the values of elastic constants are much smaller than those obtained for MoS<sub>2</sub> but are in the order of magnitude of the reported for germanene [82]. The criteria for determining the elastic stability of the hexagonal lattice are  $c_{11} > 0$ and  $c_{11} > |c_{12}|$ . In the case of the rectangular lattice, the conditions are  $c_{11} > 0$ ,  $c_{66} > 0$ , and  $c_{11}c_{22} > c_{12}^2$  [83]. Our results meet the stability criteria. Thus, both structures are elastically stable.

The mechanical properties of the 2D materials can be obtained in terms of the elastic constants as follows: the 2D shear modulus is defined as  $G = c_{66}$  and the layer modulus

is calculated with  $\gamma=(c_{11}+c_{22}+2c_{12})/4$ . The 2D Young's moduli (in-plane stiffness) for strains in the Cartesian [10] and [01] directions are  $Y_{[10]}=(c_{11}c_{22}-c_{12}^2)/c_{22}$ , and  $Y_{[01]}=(c_{11}c_{22}-c_{12}^2)/c_{11}$ . The corresponding 2D Poisson's ratio in the [10] and [01] directions are obtained with:  $\nu_{[10]}=c_{12}/c_{22}$ , and  $\nu_{[01]}=c_{12}/c_{11}$ . The results are listed in Table 3. Unlike the 1T and 2H phases, the 1T' presents a directional dependence of the mechanical properties due to its crystal structure.

In order to observe the anisotropy and the differences in the mechanical properties between 1T and 1T' phases, we have plotted in Fig. 8 the angular dependence of (a) G, (b) Y, and (c) v by using the ElATools code [77]. The shape of G, Y, and v for phase 1T indicates the elastic isotropy, where the directional values are listed in Table 3. In the case of phase 1T'  $G_{\text{max}}$  ( $G_{\text{min}}$ ) = 14.36 (10.32) N/m for  $\phi$  = 44.64 (0)°. The maximum of 2D Young's modulus is in the [01] direction, so  $Y_{\text{max}} = Y_{[01]} = 38.18$  N/m, and  $Y_{\text{min}} = 28.96$  N/m for  $\phi$  = 41.76°. The values obtained for  $v_{\text{max}}$  and  $v_{\text{min}}$  are 0.41 and 0.25 for  $\phi$  = 46.8 and 0°, respectively. Similar differences in the mechanical properties between 1T and 1T' phases were observed in MoS<sub>2</sub> [84].

#### 3.2.4. Magnetic properties

Effective models are one of the best approaches to account for magnetic interactions in the many-body problem. The most common effective model corresponds to the Heisenberg Hamiltonian defined in its simplest form as  $H = -\sum_{i \neq j} J_{ij} \mathbf{S}_i \cdot \mathbf{S}_j$  [85], where the sum runs through all magnetic sites i, j in the system,  $\mathbf{S}_i$  denotes the normalized spin vector at site i, and  $J_{ij}$  represents the exchange coupling constants between different magnetic sites. The  $J_{ij}$  terms allow for quantitatively predicting the magnetic properties of a material, such as its critical temperature [86], the spin-wave dynamics [85], or the relationship between its structural and magnetic degrees of freedom [87].

To obtain the exchange constants  $J_{ij}$  from first-principles calculations, the Heisenberg Hamiltonian is fitted to the total energy changes of the material due to perturbations of the magnetic ground state [88]. In figure 9 (a), we show the exchange constants as a function of the distance between

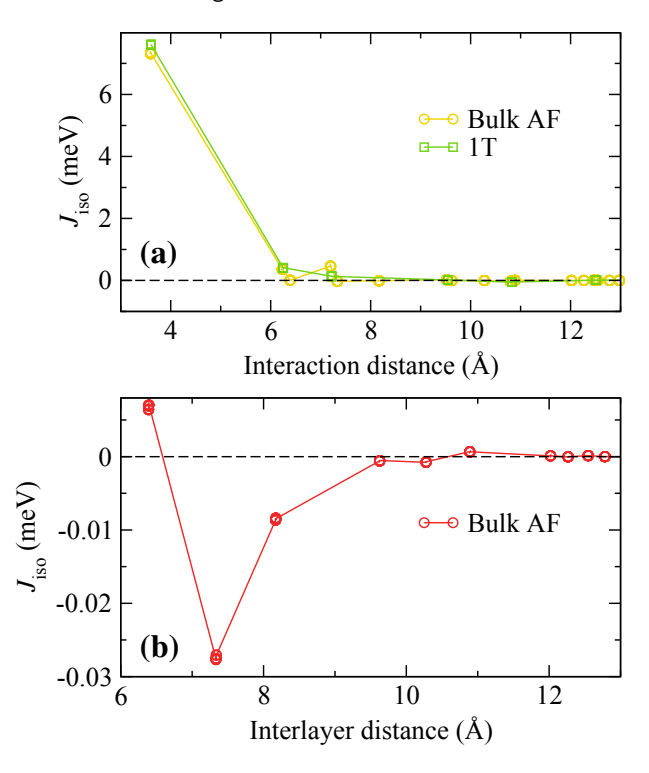


**Figure 9:** Exchange constants for bulk and 2D hexagonal FeCl. (a) Exchange constants corresponding to all interactions as functions of the interacting distance. (b) The exchange constants of the interlayer interactions in bulk  $FeCl_2$  as a distance function.

magnetic sites up to an interacting distance of  $12\ \text{Å}$  (the values for greater distances were found to be negligible as it is expected for the exchange interaction).

We found that the nearest-neighbor interaction dominates the magnetic properties in all considered cases since its energy value is considerably more significant than the rest. Additionally, the values of all the intralayer exchange constants are positive for all cases, which denotes the inplane FM nature of both systems [89]. A difference of less than 0.3 meV is observed between the in-plane exchange constants of the bulk and the 2D layer. This slight difference is also observed when introducing the vdW correction in the bulk material. We observed tiny differences in the results of phase 1T and 1T' for exchange constants; therefore, we only discuss the results from the 1T phase here. Later, we will see the difference between both phases by analyzing the magnetic anisotropy energy (MAE).

To dig deeper into the effect of the vdW forces on the magnetic properties of the bulk, we varied the distance between layers and recalculated the exchange constants. In Fig. 9 (b), we show the exchange constant of the nearest neighbor interaction as a function of the spacing between the Fe atoms belonging to neighbor layers. The exchange constants corresponding to the interlayer interactions are primarily negative, which suggests the AFM alignment between different layers.

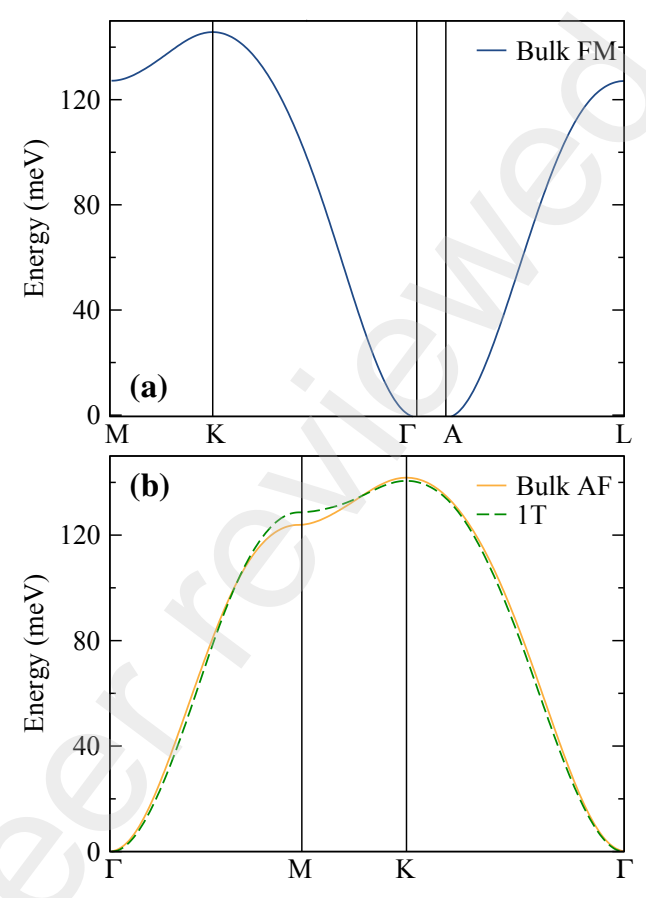


**Figure 10:** Magnon dispersion for bulk and 2D hexagonal FeCl<sub>2</sub>. **(a)** Magnon energies of the FM configuration of bulk FeCl<sub>2</sub> **(b)** Comparison of the magnon dispersion of FeCl <sub>2</sub>monolayer and AFM FeCl<sub>2</sub> bulk.

The exchange constants can be used to compute the magnon energies from which we can gain information about the systems. In this work, we used the Linear Spin-Wave Theory (LSWT) [90] as the method to compute the magnon energies. First, we compute the magnon dispersion of the FM bulk  $FeCl_2$  and find that it has a global minimum at the point A = (0.0, 0.0, 0.5), see Fig. 10 (a); this implies that the magnetic configuration generated by this propagation vector is more stable. In fact, the generated AFM structure is the one reported experimentally [91, 92]. Then, we compute the magnon energies of the monolayer and compare them with the AFM bulk, see Fig. 10 (b). In both cases, they have a global minimum at the  $\Gamma$  point, which implies the stability of their magnetic configuration.

To explore the FM nature of our structures in more detail, we used the exchange constants to obtain temperature-dependent magnetization. This was done by running Metropolis Monte-Carlo simulations within the Vampire code [93]. We considered interactions up to 12 Å and used a 40×40 supercell for the mono-layer. Our main results are contained in Fig. 11. The Curie temperature,  $T_{\rm C}$ , was obtained by fitting our data to the classical Curie-Bloch equation  $M(T) = M_S [1 - (T/T_{\rm C})^\alpha]^\beta$ , where  $M_S$  is the spontaneous magnetization. This equation gives us a Curie temperature

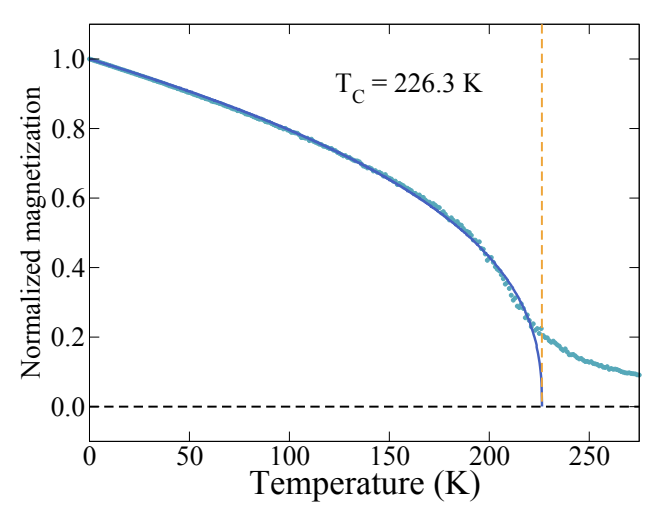


Figure 11: Dependence of the relative magnetization on the temperature for the FM 2D FeCl $_2$ . The estimated Curie temperature was 226.3 K.

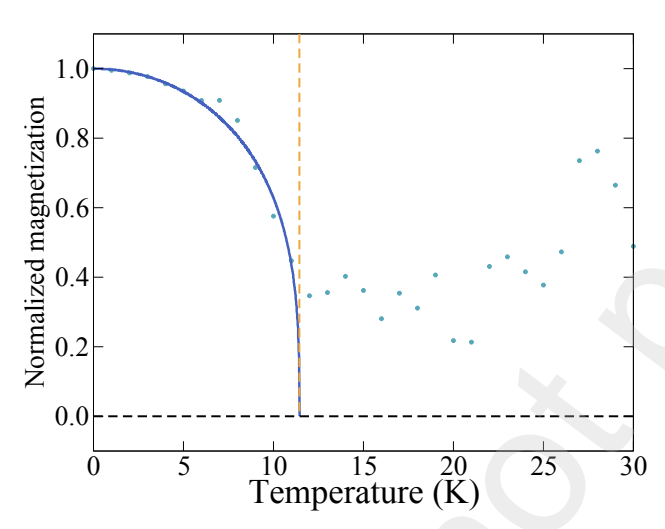
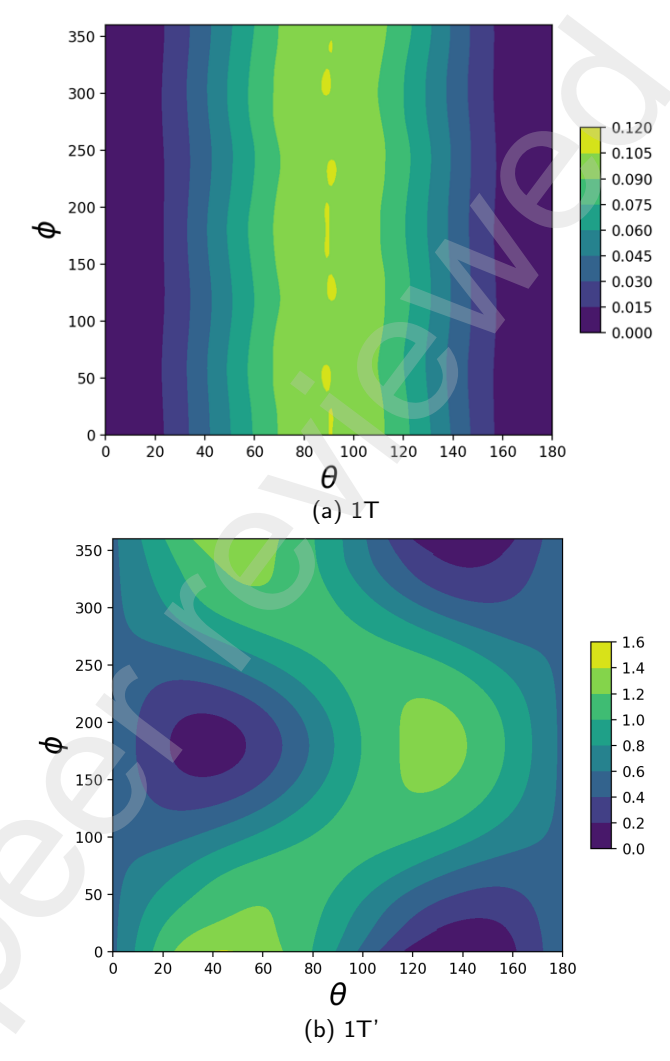


Figure 12: Magnetization of the antiparallel aligned magnetic species as a function of temperature for the AFM bulk FeCl<sub>2</sub>.

of 226.3 K for the 2D system ( $\alpha = 0.98$ ,  $\beta = 0.39$ ), which is close to the value obtained for the 2H phase of FeCl<sub>2</sub> ( $T_{\rm C} = 260$  K) [94]. Despite the slight differences between the intra-layer exchange constants of the bulk and 2D materials, the FM character of the bulk system disappears as soon as the temperature rises above 0 K.

We also performed Monte-Carlo simulations to obtain the critical temperature for the case where an AFM configuration is considered for the bulk, as seen in Fig. 12. In this case, we observe the mean magnetization of the different magnetic ions that align themselves antiparallel to each other. The magnetization change at around 11.4 K ( $\alpha = 2.07$ ,  $\beta = 0.32$ ) suggests a phase transition at that point. The experimental value reported in the literature was 23 K [95].

To complement our study of the magnetic properties, we have computed the MAE to unveil the magnetic differences of the 1T and 1T' phases. The study of magnetic



**Figure 13:** Contour plots for the angular dependence of magnetic anisotropy energy for the unit cell made out of two magnetic atoms for the FM (a) 1T and (b) 1T' structures. Angles are given in degrees; the energy values are in meV and shown in the lateral bars.

anisotropy is particularly important since it offers relevant information for technological applications in currently active fields such as spintronics and molecular magnetism [96, 97]. The MAE, rising as a result of the crystal field (i.e., spinorbit interaction), can be obtained, employing DFT methods, by computing the energy differences as a function of the polar  $(\theta)$  and azimuthal  $(\phi)$  angles, within a fine mesh. In this work, the reference frame is formed by the axis perpendicular to the monolayer as the z axis, and the [100] direction as the x axis, and the related angles are considered in the ranges  $\theta$ :  $[0, \pi]$  and  $\phi$ :  $[0, 2\pi]$ .

Figure 13 shows the angular dependence of MAE for the (a) 1T and (b) 1T' systems. As observed, very different behaviors are obtained for the two systems. MAE's  $\phi$  dependence is barely noted in the first case. The gross angular dependence relies on the polar angle, which exhibits an uniaxial anisotropy axis perpendicular to the surface. This uniaxial anisotropy can be well described by  $E_{K1}$  ( $\theta$ ) =

 $K_1 sin^2 \theta$ , with anisotropy constant  $K_1 = 0.05$  meV/atom. Thus, the 1T structure exhibits a FM configuration whose orientation is perpendicular to the surface plane.

On the other hand, the 1T' structure exhibits a uniaxial anisotropy as well, with relative minima located at  $(\theta, \phi)$ =  $(140^{\circ}, 0^{\circ})$  and  $(40^{\circ}, 180^{\circ})$ . For this case, the relative maxima is located at (50°, 0°) and (130°, 180°). Unlike the previous case, a magnetization reversal occurs by overcoming an energy barrier of 0.49 meV/atom, which is an order of magnitude higher than the symmetric case, instead of going through the maximum points. Therefore, in this case, the fundamental magnetic state is a FM configuration oriented along the easy axis of magnetization given by  $(\theta,$  $\phi$ ) = (40°, 0°) out of the surface. This anisotropy energy can be, phenomenologically, written as  $E_{K2}(\theta, \phi) = K_2$  $\sin^2(\theta - 140)\sin^2(\phi)$ , with  $K_2 = 0.49$  meV/atom. Since the 1T' system presents a MAE value above the symmetric one, its magnetic configuration exhibits higher stability under external magnetic fields.

#### 4. Conclusions

In summary, we have used first-principles calculations based on GGA+U and an appropriate vdW approximation to successfully characterize the crystalline structure and the electronic, mechanical, vibrational, and magnetic properties of bulk FeCl<sub>2</sub>. This methodology was also used to compute the same properties of the 2D 1T and 1T' systems of FeCl<sub>2</sub>. Our results agree with the recent experimental outcomes reported in the literature for the 1T structure. Furthermore, we found that the three arrangements are elastic and dynamically stable, where our results are in better agreement with the experimental values than previous theoretical reports, which validates our procedure beyond only determining the structure stability. Furthermore, the magnetic characterization reaffirms the FM nature of the 2D 1T structure and puts in perspective the differences with the 1T' in the MAE due to the anisotropy given by their structural differences. In this sense, it is remarkable to mention the electronic differences between the 1T (half-metal) and 1T' (semiconductor) phases, which could open the door to performing new studies on this subject. Also, we observed some differences in the elastic and mechanical properties due to the elastic anisotropies.

We strongly believe that our procedure could be successfully used to study other TMDH such as FeBr<sub>2</sub>, VCl<sub>2</sub>, and VBr<sub>2</sub>, for which experimental results from bulk and phase 1T are already available.

#### 5. acknowledgments

S. L.-M. thanks CONACYT of Mexico for financial support through the program "Programa de Investigadoras e Investigadores por México". E.E. H.-V. acknowledges to the program "Estancias Posdoctorales por México, CONCAYT, ID: 0000-0001-7340-6456. J.M.L. thanks for the support of the project ANID/CONICYT FONDECYT grant no.

1210193, and by the Millennium Institute on Green Ammonia as Energy Vector - MIGA (ICN2021-023) supported by the Millennium Scientific Initiative by the Agencia Nacional de Investigación y Desarrollo (ANID) (Chile). Research performed at West Virginia University was supported by the U.S. Department of Energy (DOE), Office of Science, Basic Energy Sciences (BES), under Award DE-SC0021375 (implementation and computational studies for the magnetic properties). The authors gratefully acknowledge the computing time granted by LANCAD and CONACYT on the supercomputer Miztli at LSVP DGTIC UNAM. Also, the IPICYT Supercomputing National Center for Education & Research grant TKII-R2024-SLM1/EEHV. We thank the Pittsburgh Supercomputer Center (Bridges2) and San Diego Supercomputer Center (Expanse) through allocation DMR140031 from the Advanced Cyberinfrastructure Coordination Ecosystem: Services & Support (ACCESS) program, which is supported by National Science Foundation grants #2138259, #2138286, #2138307, #2137603, and #2138296. We also recognize the computational resources provided by the WVU Research Computing Dolly Sods HPC cluster, which is funded in part by NSF OAC-2117575.

#### **CRediT** authorship contribution statement

Sinhué López-Moreno: Supervision, Methodology, Calculations, Writing - Original Draft, Editing. Andres Tellez-Mora: Calculations, Writing. Jose Mejía-López: Calculations, Writing. Esther Elena Hernández-Vázquez: Calculations, Writing. Aldo H. Romero: Conceptualization, Writing. Jose Luis Morán-López: Conceptualization, Writing, Editing.

#### References

- [1] A. H. Castro Neto, F. Guinea, N. M. R. Peres, K. S. Novoselov, A. K. Geim, Rev. Mod. Phys. 81 (2009) 109–162. doi:10.1103/RevModPhys. 81.109.
- [2] Y. Zhang, L. Zhang, T. Lv, P. K. Chu, K. Huo, ChemSusChem 13 (2020) 1114–1154. doi:10.1002/cssc.201903245.
- [3] C. Gong, X. Zhang, Science 363 (2019) eaav4450. doi:10.1126/ science.aav4450.
- [4] Y. Liu, N. Weiss, X. Duan, C. Hung-Chieh, Y. Huang, X. Duan, Nat. Rev. Mater. 1 (2016) 16042. doi:10.1038/natrevmats.2016.42.
- [5] K. S. Novoselov, A. Mishchenko, A. Caralho, A. H. Castro-Neto, Science 353 (2016) 6298. doi:10.1126/science.aac9439.
- [6] Y. Wang, J. C. Kim, R. J. Wu, J. Martinez, X. Song, J. Yang, F. Zhao, A. Mkhoyan, Nature 568 (2019) 70. doi:10.1038/s41586-019-1052-3.
- [7] E. Kovaleva, I. Melchakova, N. Mikhaleva, F. Tomilin, S. Ovchinnikov, W. Baek, V. Pomogaev, P. Avramov, A. Kuzubov, J. Phys. Chem. Solids 134 (2019) 324–332. doi:10.1016/j.jpcs.2019.05.036.
- [8] C. Vettier, W. Yelon, J. Phys. Chem. Solids 36 (1975) 401–405. doi:10.1016/0022-3697(75)90065-7.
- [9] D. L. Duong, S. J. Yun, Y. H. Lee, ACS Nano 11 (2017) 11803–11830. doi:10.1021/acsnano.7b07436.
- [10] S. Cai, F. Yang, C. Gao, Nanoscale 12 (2020) 16041–16045. doi:10.1039/D0NR03128C.
- [11] Q. H. Wang, A. Bedoya-Pinto, M. Blei, A. H. Dismukes, A. Hamo, S. Jenkins, M. Koperski, Y. Liu, Q.-C. Sun, E. J. Telford, H. H. Kim, M. Augustin, U. Vool, J.-X. Yin, L. H. Li, A. Falin, C. R. Dean, F. Casanova, R. F. L. Evans, M. Chshiev, A. Mishchenko,

- C. Petrovic, R. He, L. Zhao, A. W. Tsen, B. D. Gerardot, M. Brotons-Gisbert, Z. Guguchia, X. Roy, S. Tongay, Z. Wang, M. Z. Hasan, J. Wrachtrup, A. Yacoby, A. Fert, S. Parkin, K. S. Novoselov, P. Dai, L. Balicas, E. J. G. Santos, ACS Nano 16 (2022) 6960–7079. doi:10.1021/acsnano.1c09150.
- [12] X. Zhou, B. Brzostowski, A. Durajski, M. Liu, J. Xiang, T. Jiang, Z. Wang, S. Chen, P. Li, Z. Zhong, A. Drzewiński, M. Jarosik, R. Szczęśniak, T. Lai, D. Guo, D. Zhong, J. Phys. Chem. C 124 (2020) 9416–9423. doi:10.1021/acs.jpcc.0c03050.
- [13] S. Jiang, G. Wang, H. Deng, K. Liu, Q. Yang, E. Zhao, L. Zhu, W. Guo, J. Yang, C. Zhang, H. Wang, X. Zhang, J.-F. Dai, G. Luo, Y. Zhao, J. Lin, ACS Nano 17 (2023) 363–371. doi:10.1021/acsnano.2c08693.
- [14] E. Torun, H. Sahin, S. K. Singh, F. M. Peeters, Appl. Phys. Lett. 106 (2015) 192404. doi:10.1063/1.4921096.
- [15] M. Ashton, D. Gluhovic, S. B. Sinnott, J. Guo, D. A. Stewart, R. G. Hennig, Nano Lett. 17 (2017) 5251–5257. doi:10.1021/acs.nanolett. 7b01367.
- [16] A. A. Kistanov, S. A. Shcherbinin, R. Botella, A. Davletshin, W. Cao, J. Phys. Chem. Lett. 13 (2022) 2165–2172. doi:10.1021/acs.jpclett. 2c00367.
- [17] D. Lu, L. Liu, Y. Ma, K. Yang, H. Wu, J. Mater. Chem. C 10 (2022) 8009–8014. doi:10.1039/D2TC00554A.
- [18] Q. Yao, J. Li, Q. Liu, Phys. Rev. B 104 (2021) 035108. doi:10.1103/ PhysRevB.104.035108.
- [19] E. Ceyhan, M. Yagmurcukardes, F. M. Peeters, H. Sahin, Phys. Rev. B 103 (2021) 014106. doi:10.1103/PhysRevB.103.014106.
- [20] G. Benedek, A. Frey, Phys. Rev. B 21 (1980) 2482–2498. doi:10.1103/ PhysRevB.21.2482.
- [21] W. Yelon, R. Scherm, C. Vettier, Solid State Commun. 15 (1974) 391–394. doi:10.1016/0038-1098(74)90783-2.
- [22] G. Gorodetsky, A. Shaulov, V. Volterra, J. Makovsky, Phys. Rev. B 13 (1976) 1205–1208. doi:10.1103/PhysRevB.13.1205.
- [23] R. J. Birgeneau, W. B. Yelon, E. Cohen, J. Makovsky, Phys. Rev. B 5 (1972) 2607–2615. doi:10.1103/PhysRevB.5.2607.
- [24] K. Momma, F. Izumi, J. Appl. Crystallog. 44 (2011) 1272–1276. doi:10.1107/S0021889811038970.
- [25] P. E. Blöchl, Phys. Rev. B 50 (1994) 17953–17979. doi:10.1103/ PhysRevB.50.17953.
- [26] G. Kresse, D. Joubert, Phys. Rev. B 59 (1999) 1758–1775. doi:10.1103/PhysRevB.59.1758.
- [27] G. Kresse, J. Hafner, Phys. Rev. B 47 (1993) 558–561. doi:10.1103/ PhysRevB.47.558.
- [28] G. Kresse, J. Hafner, Phys. Rev. B 49 (1994) 14251–14269. doi:10. 1103/PhysRevB.49.14251.
- [29] G. Kresse, J. Furthmüller, Comput. Mater. Sci. 6 (1996) 15. doi:10. 1016/0927-0256(96)00008-0.
- [30] G. Kresse, J. Furthmüller, Phys. Rev. B 54 (1996) 11169–11186. doi:10.1103/PhysRevB.54.11169.
- [31] J. P. Perdew, K. Burke, M. Ernzerhof, Phys. Rev. Lett. 77 (1996) 3865–3868. doi:10.1103/PhysRevLett.77.3865.
- [32] S. L. Dudarev, G. A. Botton, S. Y. Savrasov, C. J. Humphreys, A. P. Sutton, Phys. Rev. B 57 (1998) 1505–1509. doi:10.1103/PhysRevB.57. 1505
- [33] S. López-Moreno, A. H. Romero, J. Mejía-López, A. Muñoz, I. V. Roshchin, Phys. Rev. B 85 (2012) 134110. doi:10.1103/PhysRevB.85.
- [34] J. A. Barreda-Argüeso, S. López-Moreno, M. N. Sanz-Ortiz, F. Aguado, R. Valiente, J. González, F. Rodríguez, A. H. Romero, A. Muñoz, L. Nataf, F. Baudelet, Phys. Rev. B 88 (2013) 214108. doi:10.1103/PhysRevB.88.214108.
- [35] S. López-Moreno, A. H. Romero, J. Mejía-López, A. Muñoz, Phys. Chem. Chem. Phys. 18 (2016) 33250–33263. doi:10.1039/C6CP05467F.
- [36] S. López, A. H. Romero, J. Mejía-López, J. Mazo-Zuluaga, J. Restrepo, Phys. Rev. B 80 (2009) 085107. doi:10.1103/PhysRevB.80.085107.

- [37] S. López-Moreno, D. Errandonea, J. Pellicer-Porres, D. Martínez-García, S. J. Patwe, S. N. Achary, A. K. Tyagi, P. Rodríguez-Hernández, A. Muñoz, C. Popescu, Inorg. Chem. 57 (2018) 7860–7876. doi:10.1021/acs.inorgchem.8b00984.
- [38] J. Mejía-López, J. Mazo-Zuluaga, S. López-Moreno, F. Muñoz, L. F. Duque, A. H. Romero, Phys. Rev. B 90 (2014) 035411. doi:10.1103/PhysRevB.90.035411.
- [39] J. Ruiz-Fuertes, D. Errandonea, S. López-Moreno, J. González, O. Gomis, R. Vilaplana, F. J. Manjón, A. Muñoz, P. Rodríguez-Hernández, A. Friedrich, I. A. Tupitsyna, L. L. Nagornaya, Phys. Rev. B 83 (2011) 214112. doi:10.1103/PhysRevB.83.214112.
- [40] P. B. Romero-Vázquez, S. López-Moreno, D. Errandonea, Crystals 12 (2022) 1835. doi:10.3390/cryst12121835.
- [41] J. Gonzalez-Platas, S. López-Moreno, E. Bandiello, M. Bettinelli, D. Errandonea, Inorg. Chem. 59 (2020) 6623–6630. doi:10.1021/acs. inorgchem.0c00772.
- [42] D. Diaz-Anichtchenko, J. E. Aviles-Coronado, S. López-Moreno, R. Turnbull, F. J. Manjón, C. Popescu, D. Errandonea, Inorg. Chem. 63 (2024) 6898–6908. doi:10.1021/acs.inorgchem.4c00345.
- [43] S. Grimme, J. Comput. Chem. 27 (2006) 1787–1799. doi:10.1002/jcc.20495.
- [44] S. Grimme, J. Antony, S. Ehrlich, H. Krieg, J. Chem. Phys. 132 (2010) 154104. doi:10.1063/1.3382344.
- [45] A. Tkatchenko, M. Scheffler, Phys. Rev. Lett. 102 (2009) 073005. doi:10.1103/PhysRevLett.102.073005.
- [46] T. Bucko, S. Lebegue, J. Hafner, J. G. Angyan, J. Chem. Theory Comput. 9 (2013) 4293–4299. doi:10.1021/ct400694h.
- [47] M. Dion, H. Rydberg, E. Schröder, D. C. Langreth, B. I. Lundqvist, Phys. Rev. Lett. 92 (2004) 246401. doi:10.1103/PhysRevLett.92. 246401.
- [48] G. Román-Pérez, J. M. Soler, Phys. Rev. Lett. 103 (2009) 096102. doi:10.1103/PhysRevLett.103.096102.
- [49] J. Klimeš, D. R. Bowler, A. Michaelides, J. Phys.: Condens. Matter 22 (2010) 022201. doi:10.1088/0953-8984/22/2/022201.
- [50] K. Lee, E. D. Murray, L. Kong, B. I. Lundqvist, D. C. Langreth, Phys. Rev. B 82 (2010) 081101. doi:10.1103/PhysRevB.82.081101.
- [51] J. c. v. Klimeš, D. R. Bowler, A. Michaelides, Phys. Rev. B 83 (2011) 195131. doi:10.1103/PhysRevB.83.195131.
- [52] T. Thonhauser, V. R. Cooper, S. Li, A. Puzder, P. Hyldgaard, D. C. Langreth, Phys. Rev. B 76 (2007) 125112. doi:10.1103/PhysRevB.76. 125112
- [53] I. Hamada, Phys. Rev. B 89 (2014) 121103. doi:10.1103/PhysRevB.89.
- [54] H. J. Monkhorst, J. D. Pack, Phys. Rev. B 13 (1976) 5188–5192. doi:10.1103/PhysRevB.13.5188.
- [55] K. Parlinski, Computer Code PHONON. See: http://wolf.ifj.edu.pl/phonon, 2008.
- [56] Y. Le Page, P. Saxe, Phys. Rev. B 65 (2002) 104104. doi:10.1103/ PhysRevB.65.104104.
- [57] S. Singh, L. Lang, V. Dovale-Farelo, U. Herath, P. Tavadze, F.-X. Coudert, A. H. Romero, Comp. Phys. Commun. 267 (2021) 108068. doi:10.1016/j.cpc.2021.108068.
- [58] J. M. Soler, E. Artacho, J. D. Gale, A. García, J. Junquera, P. Ordejón, D. Sánchez-Portal, J. Phys.: Condens. Matter 14 (2002) 2745–2779. doi:10.1088/0953-8984/14/11/302.
- [59] A. Tellez-Mora, X. He, E. Bousquet, L. Wirtz, A. H. Romero, npj Comput. Mater. 10 (2024) 20. doi:10.1038/s41524-024-01202-z.
- [60] X. He, N. Helbig, M. J. Verstraete, E. Bousquet, Comput. Phys. Commun. 264 (2021) 107938. doi:10.1016/j.cpc.2021.107938.
- [61] M. van Setten, M. Giantomassi, E. Bousquet, M. Verstraete, D. Hamann, X. Gonze, G.-M. Rignanese, Comput. Phys. Commun. 226 (2018) 39–54. doi:10.1016/j.cpc.2018.01.012.
- [62] J. Klimeš, D. R. Bowler, A. Michaelides, J. Phys.: Condens. Matter 22 (2009) 022201. doi:10.1088/0953-8984/22/2/022201.
- [63] I. W. Johnstone, D. J. Lockwood, G. Mischler, J. Phys. C: Solid State Phys. 11 (1978) 2147–2164. doi:10.1088/0022-3719/11/10/025.
- [64] S. Grimme, S. Ehrlich, L. Goerigk, J. Comput. Chem. 32 (2011) 1456–1465. doi:10.1002/jcc.21759.

- [65] A. Tkatchenko, R. A. DiStasio, R. Car, M. Scheffler, Phys. Rev. Lett. 108 (2012) 236402. doi:10.1103/PhysRevLett.108.236402.
- [66] S. Singh, C. Espejo, A. H. Romero, Phys. Rev. B 98 (2018) 155309. doi:10.1103/PhysRevB.98.155309.
- [67] J. Thomas, G. Jezequel, I. Pollini, J. Phys.: Condens. Matter 2 (1990) 5439–5453. doi:10.1088/0953-8984/2/24/015.
- [68] M. K. Wilkinson, J. W. Cable, E. O. Wollan, W. C. Koehler, Phys. Rev. 113 (1959) 497–507. doi:10.1103/PhysRev.113.497.
- [69] A. G. Every, A. K. McCurdy, Table 16. trigonal system, 6 constants, 1992. doi:10.1007/10046537\_25, copyright 1992 Springer-Verlag Berlin Heidelberg.
- [70] J. Nye, P. Nye, Physical Properties of Crystals: Their Representation by Tensors and Matrices, Oxford science publications, Clarendon Press, 1985. URL: https://books.google.com.mx/books?id=ugwql-uVB44C.
- [71] F. Mouhat, F. m. c.-X. Coudert, Phys. Rev. B 90 (2014) 224104. doi:10.1103/PhysRevB.90.224104.
- [72] N. Najafvandzadeh, S. López-Moreno, D. Errandonea, P. Pavone, C. Draxl, Mater. Today Commun. 24 (2020) 101089. doi:10.1016/j. mtcomm.2020.101089.
- [73] P. B. Romero-Vázquez, S. López-Moreno, D. Errandonea, J. Phys. Chem. Solids 171 (2022) 110979. doi:10.1016/j.jpcs.2022.110979.
- [74] V. Wang, N. Xu, J.-C. Liu, G. Tang, W.-T. Geng, Comp. Phys. Commun. 267 (2021) 108033. doi:10.1016/j.cpc.2021.108033.
- [75] X.-Q. Chen, H. Niu, D. Li, Y. Li, Intermetallics 19 (2011) 1275–1281. doi:10.1016/j.intermet.2011.03.026.
- [76] Y. Tian, B. Xu, Z. Zhao, Int. J. Refractory Metal Hard Mater. 33 (2012) 93–106. doi:10.1016/j.ijrmhm.2012.02.021.
- [77] S. Yalameha, Z. Nourbakhsh, D. Vashaee, Comput. Phys. Commun. 271 (2022) 108195. doi:10.1016/j.cpc.2021.108195.
- [78] J.-H. Fan, Y. Qin, M. Azeem, Z.-Z. Zhang, Z.-G. Li, N. Sun, Z.-Q. Yao, W. Li, Dalton Trans. 50 (2021) 2648–2653. doi:10.1039/D0DT04165C.
- [79] G. Feng, Y. Qin, C. Ran, L. Ji, L. Dong, W. Li, APL Mater. 6 (2018) 114201. doi:10.1063/1.5042645.
- [80] J. Han, X. Chen, W. Yang, C. Lv, X. Lin, X. Wang, G. Wei, W. Zhao, J. Mater. Chem. C 10 (2022) 607–615. doi:10.1039/D1TC05094J.
- [81] K. Liu, Q. Yan, M. Chen, W. Fan, Y. Sun, J. Suh, D. Fu, S. Lee, J. Zhou, S. Tongay, J. Ji, J. B. Neaton, J. Wu, Nano Lett. 14 (2014) 5097–5103. doi:10.1021/nl501793a.
- [82] R. C. Andrew, R. E. Mapasha, A. M. Ukpong, N. Chetty, Phys. Rev. B 85 (2012) 125428. doi:10.1103/PhysRevB.85.125428.
- [83] M. Maździarz, 2D Mater. 6 (2019) 048001. doi:10.1088/2053-1583/ ab2ef3.
- [84] N. T. Hung, A. R. T. Nugraha, R. Saito, J. Phys. D: Appl. Phys. 51 (2018) 075306. doi:10.1088/1361-6463/aaa68f.
- [85] S. V. Halilov, H. Eschrig, A. Y. Perlov, P. M. Oppeneer, Phys. Rev. B 58 (1998) 293–302. doi:10.1103/PhysRevB.58.293.
- [86] I. Turek, J. Kudrnovsk, G. Bihlmayer, S. B. gel, J. Phys.: Condens. Matter 15 (2003) 2771–2782. doi:10.1088/0953-8984/15/17/327.
- [87] Y. Liu, L.-S. Xie, Z. Yuan, K. Xia, Phys. Rev. B 96 (2017) 174416. doi:10.1103/PhysRevB.96.174416.
- [88] A. Liechtenstein, M. Katsnelson, V. Antropov, V. Gubanov, J. Mag. Mag. Mater. 67 (1987) 65–74. doi:10.1016/0304-8853(87)90721-9.
- [89] M. Pajda, J. Kudrnovský, I. Turek, V. Drchal, P. Bruno, Phys. Rev. B 64 (2001) 174402. doi:10.1103/PhysRevB.64.174402.
- [90] S. Toth, B. Lake, J. Phys.: Condens. Matter 27 (2015) 166002. doi:10.
- 1088/0953-8984/27/16/166002.
- [91] P. D. F. Isles, Ecology 101 (2020) e03153. doi:10.1002/ecy.3153.
- [92] T. Y. Chuah, C. Y. Lim, R. Z. Tan, B. Pratumvinit, T. P. Loh, S. Vasikaran, C. Markus, Ann. Lab. Med. 43 (2023) 408–417. doi:10. 3343/alm.2023.43.5.408.
- [93] R. F. L. Evans, W. J. Fan, P. Chureemart, T. A. Ostler, M. O. A. Ellis, R. W. Chantrell, J. Phys.: Condens. Matter 26 (2014) 103202. doi:10.1088/0953-8984/26/10/103202.
- [94] K. Saritas, S. Ismail-Beigi, Phys. Rev. B 106 (2022) 134421. doi:10.1103/PhysRevB.106.134421.

- [95] C. Vettier, W. B. Yelon, Phys. Rev. B 11 (1975) 4700–4710. doi:10. 1103/PhysRevB.11.4700.
- [96] P. Gambardella, S. Rusponi, M. Veronese, S. S. Dhesi, C. Grazioli, A. Dallmeyer, I. Cabria, R. Zeller, P. H. Dederichs, K. Kern, C. Carbone, H. Brune, Science 300 (2003) 1130–1133. doi:10.1126/science. 1082857.
- [97] M. T. Johnson, P. J. H. Bloemen, F. J. A. den Broeder, J. J. de Vries, Rep. Prog. Phys. 59 (1996) 1409. doi:10.1088/0034-4885/59/11/002.